Electronic Supplementary Material (ESI) for Physical Chemistry Chemical Physics

Electronic Supplementary Information for:

‘Manipulating dynamics with chemical structure: Probing vibrationally-enhanced dynamics in photoexcited catechol’

Adam S. Chatterley,[a,b] Jamie D. Young,[a] Dave Townsend,[c] Justyna M. Żurek,[d]
Martin J. Paterson,[d] Gareth M. Roberts[a,]* and Vasilios G. Stavros[a,]*

[a] *Department of Chemistry, University of Warwick, Library Road, Coventry, CV4 7AL, UK*

[b] *Department of Chemistry, Durham University, South Road, Durham, DH1 3LE, UK*

[c] *Institute of Photonics & Quantum Sciences, Heriot-Watt University, Edinburgh, EH14 4AS, UK*

[d] *Institute of Chemical Sciences, Heriot-Watt University, Edinburgh, EH14 4AS, UK*

*To whom correspondence should be addressed:

g.m.roberts@warwick.ac.uk; v.stavros@warwick.ac.uk

Figures: Figs. S1 – S10

S1. Kinetic analysis of the H^+ and catechol$^+$ signal transients

Ion signal transients obtained from either time-resolved ion yield (TR-IY) or time-resolved velocity map ion imaging (TR-VMI) measurements are modelled using a combination of exponential rise and decay functions, which are convoluted with the Gaussian instrument response function, $g(\Delta t)$.

All catechol$^+$, guaiacol$^+$ and [catechol-d_2]$^+$ parent signal transients are fitted to a bi-exponential decay function, $P(\Delta t)$, which has the functionality:

$$P(\Delta t) = \left[g(\Delta t) * A\exp\left(-\frac{\Delta t}{\tau_d}\right)\right] + \left[g(\Delta t) * B\exp\left(-\frac{\Delta t}{\tau_P}\right)\right]. \quad \text{(S1)}$$

H^+ and D^+ signal transients extracted *via* integration over the range 5000 – 8000 cm^{-1} in TKER spectra (between 280.5 – 254 nm), where tunnelling dynamics are active (see Fig. S5), are fitted to a bi-exponential rise function, $H_T(\Delta t)$:

$$H_T(\Delta t) = \left[g(\Delta t) * \left\{ 1 - A\exp\left(-\frac{\Delta t}{\tau_\mathrm{r}} \right) \right\} \right] + \left[g(\Delta t) * \left\{ 1 - B\exp\left(-\frac{\Delta t}{\tau_\mathrm{T}} \right) \right\} \right]. \tag{S2}$$

Across the range 250 – 243 nm, H^+ signal transients (over 5000 – 8000 cm^{-1}) display a ‘spike’ in H^+ signal at $\Delta t = 0$ which then rapidly decays within the instrument response (~120 fs). This feature is a result of undesired multiphoton processes, which generate and ionise neutral H-atoms at the temporal overlap of both the pump and probe pulses, and increases in amplitude as the pump wavelength is tuned closer to 243 nm (see Fig. S5). To account for this, these transients are fitted using a modified version of eqn (S2), $H_{T'}(\Delta t)$, which contains an additional exponential decay function:

$$\begin{aligned} H_{T'}(\Delta t) = &\left[g(\Delta t) * \left\{ 1 - A\exp\left(-\frac{\Delta t}{\tau_\mathrm{r}} \right) \right\} \right] + \left[g(\Delta t) * \left\{ 1 - B\exp\left(-\frac{\Delta t}{\tau_\mathrm{T}} \right) \right\} \right] \\ &+ \left[g(\Delta t) * C\exp\left(-\frac{\Delta t}{\tau_\mathrm{m}} \right) \right]. \end{aligned} \tag{S3}$$

Finally, H^+ signal transients generated *via* integration over the range 10000 – 14000 cm^{-1}, between 254 – 237 nm (Fig. S6), are fitted using an exponential rise and decay function, $H_{CI}(\Delta t)$:

$$H_{CI}(\Delta t) = \left[g(\Delta t) * \left\{ 1 - A\exp\left(-\frac{\Delta t}{\tau_\mathrm{CI}} \right) \right\} \right] + \left[g(\Delta t) * B\exp\left(-\frac{\Delta t}{\tau_\mathrm{m}} \right) \right]. \tag{S4}$$

S2. Orbital hypersurfaces

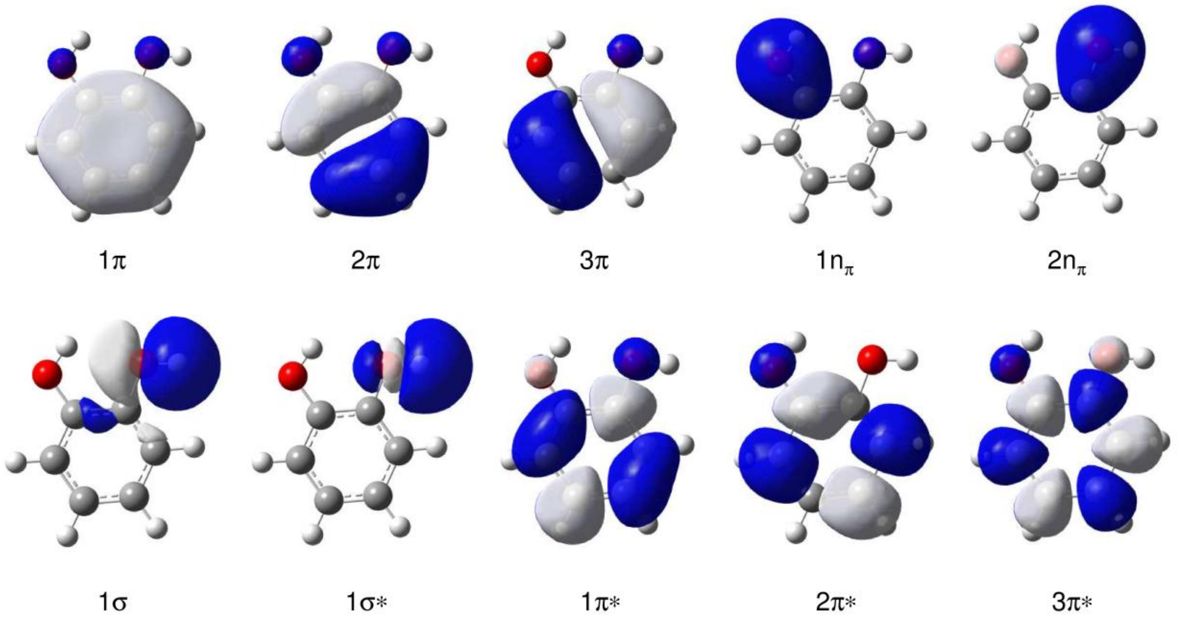

Fig. S1 Hypersurfaces of orbitals used in CASPT2 and CASSCF calculations. All presented orbitals are used in the (12,10) active space for CASPT2 calculations, while the three π, two n$_\pi$ and three π* orbitals are used in a reduced (10,8) active space for CASSCF calculations of the $S_{1\ \mathrm{min}}$ structure.

S3. Power dependence studies at $S_1(v = 0)$: λ = 280.5 nm

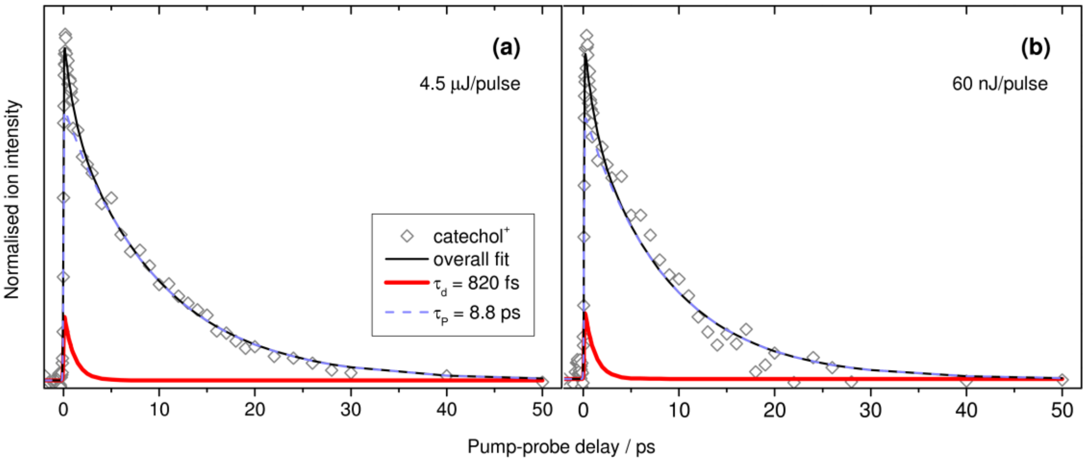

Fig. S2 Catechol$^+$ parent ion signal transients (grey diamonds) obtained following excitation at 280.5 nm with pump pulse energies of (a) 4.5 μJ/pulse and (b) 60 nJ/pulse. Overall kinetic fits using eqn (S1) are shown by the black lines. The individual fit components associated with the τ_d and τ_P time constants are shown by the bold red and dashed blue lines, respectively. No change to the amplitude of the τ_d component is observed upon reducing the power density of the pump to ~1×10^{10} W cm^{-2}.

S4. Vapour-phase UV absorption spectrum of guaiacol

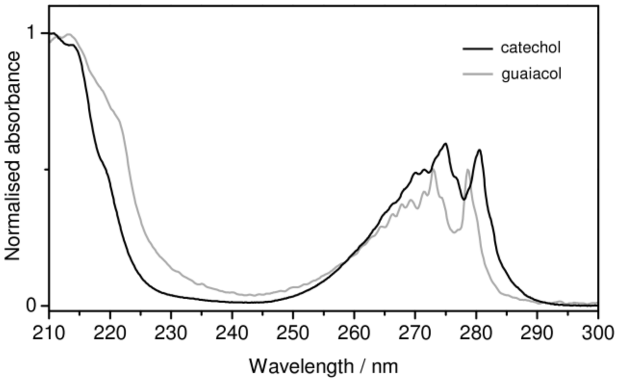

Fig. S3 Vapour-phase UV absorption spectrum of guaiacol (grey) recorded over the range 210 – 300 nm. The $S_1(v = 0)$ origin band of guaiacol is determined to lie at ~278 nm.[1, 2] The vapour-phase UV absorption spectrum of catechol is shown for comparison (black).

S5. Catechol$^+$ parent ion signal transients: λ = 280.5 – 237 nm

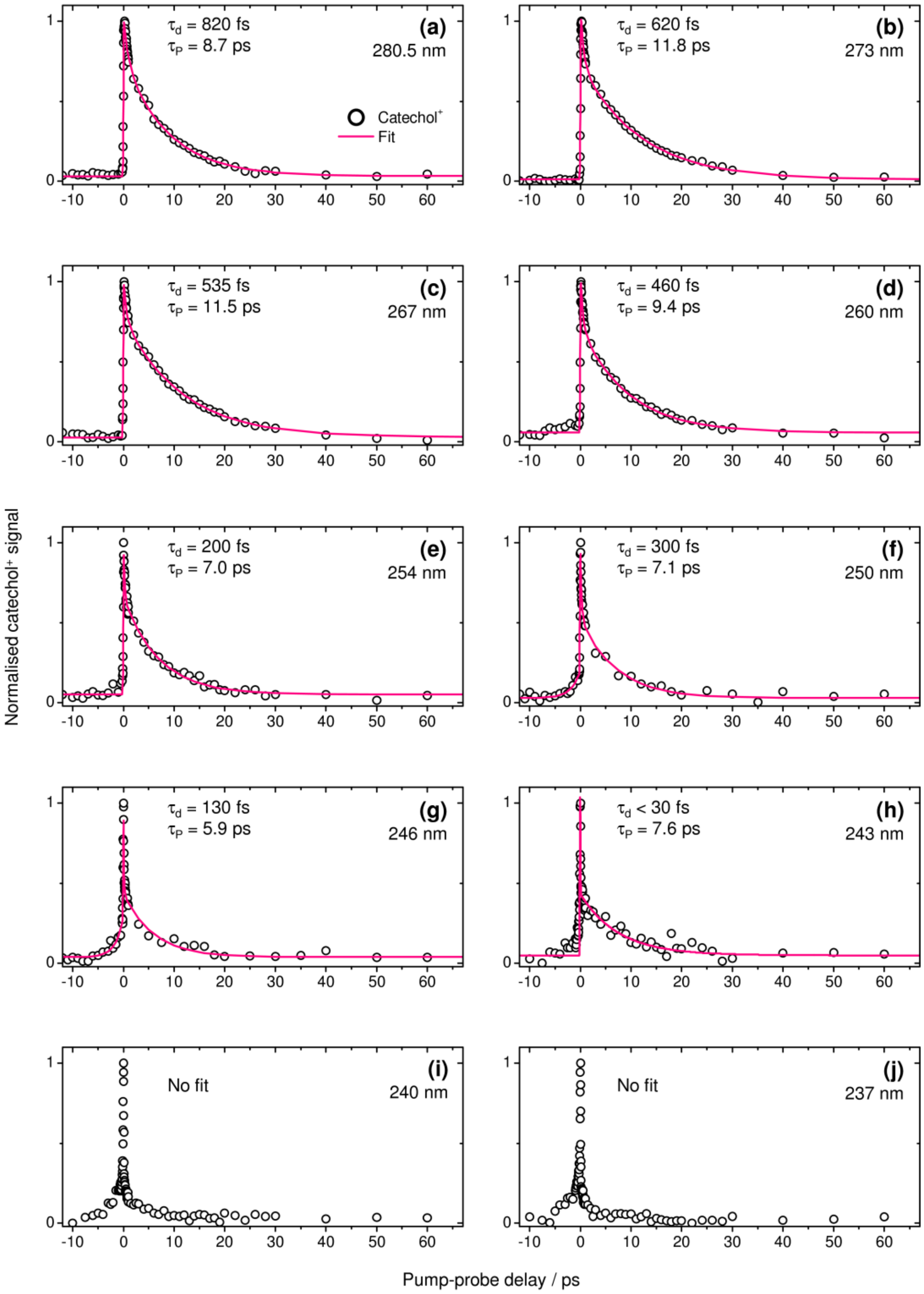

Fig. S4 Catechol$^+$ parent ion signal transients (open circles) recorded at many wavelengths over the range 280.5 – 237 nm. Associated kinetic fits to the data using eqn (S1) are indicated by the pink lines. Extracted time constants at each excitation wavelength are also provided.

S6. H$^+$ signal transients (5000 – 8000 cm^{-1}): λ = 280.5 – 243 nm

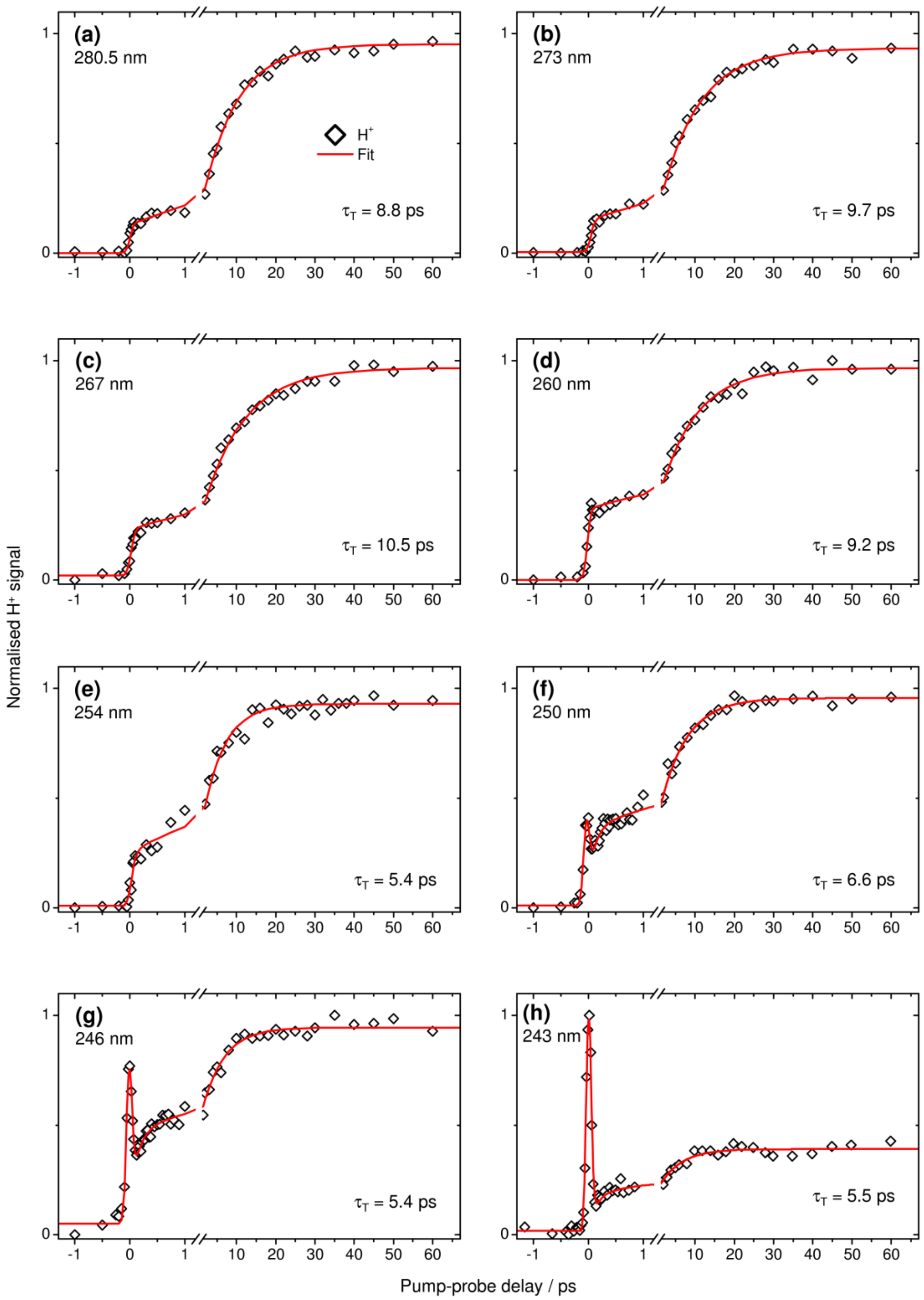

Fig. S5 H$^+$ signal transients obtained by integrating signal in TKER spectra over the range 5000 – 8000 cm^{-1} at many Δt (open diamonds), over the excitation wavelength range 280.5 – 243 nm (where tunnelling dynamics are observed to be active). Kinetic fits to the transients using eqn (S2) (280.5 – 254 nm) and eqn (S3) (250 – 243 nm) are indicated by the red lines. Extracted τ_T time constants are also provided.

S7. H^+ signal transients (10000 – 14000 cm^{-1}): λ = 254 – 237 nm

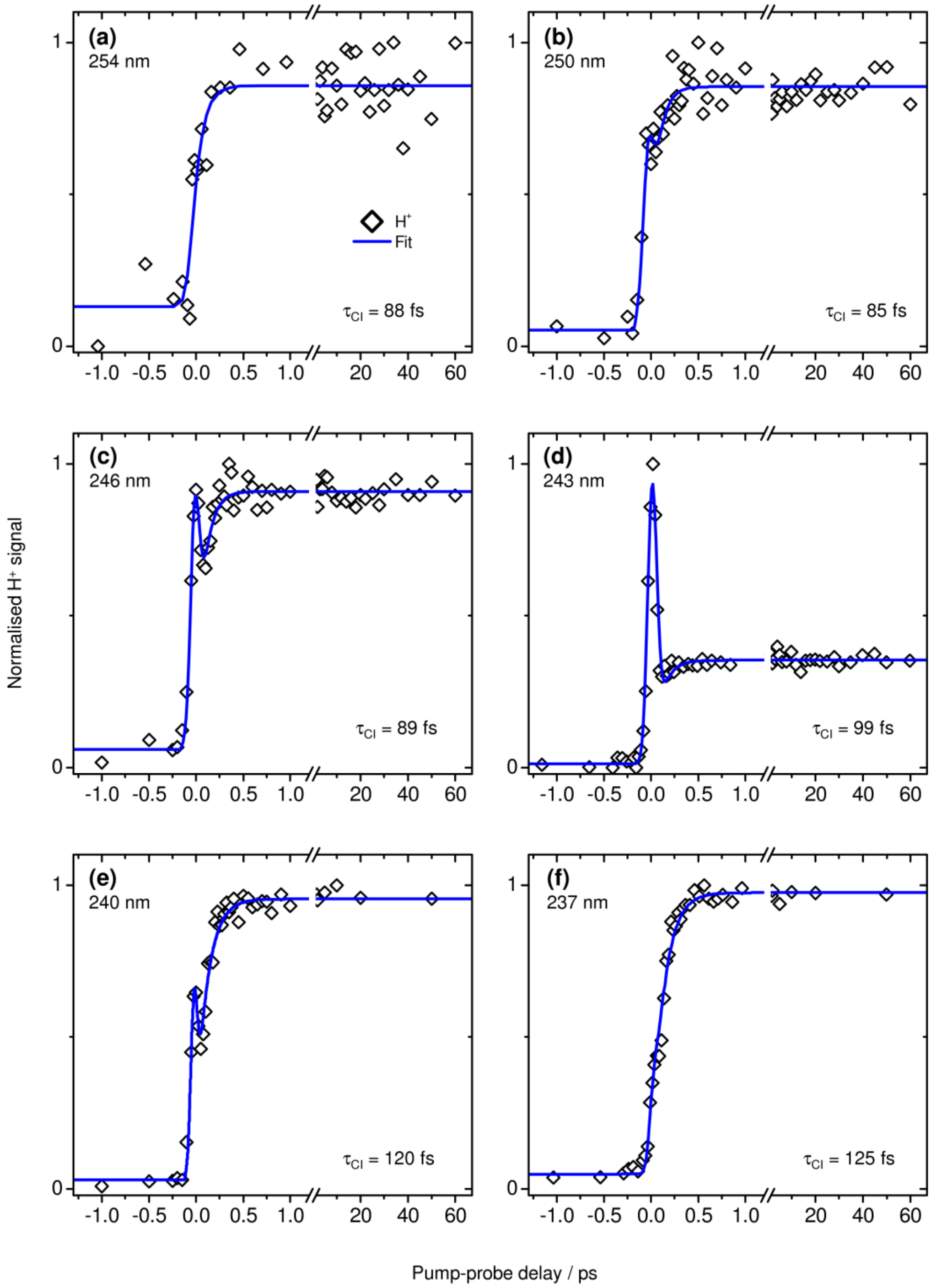

Fig. S6 H^+ signal transients obtained by integrating signal in TKER spectra over the range 10000 – 14000 cm^{-1} at many Δt (open diamonds), over the excitation wavelength range 254 – 237 nm (where ultrafast O^1-H fission dynamics are observed to be active). Kinetic fits to the transients using eqn (S4) are indicated by the blue lines. Extracted τ_{CI} time constants are also provided.

S8. Vibrational modes of catechol's S_1 excited electronic state

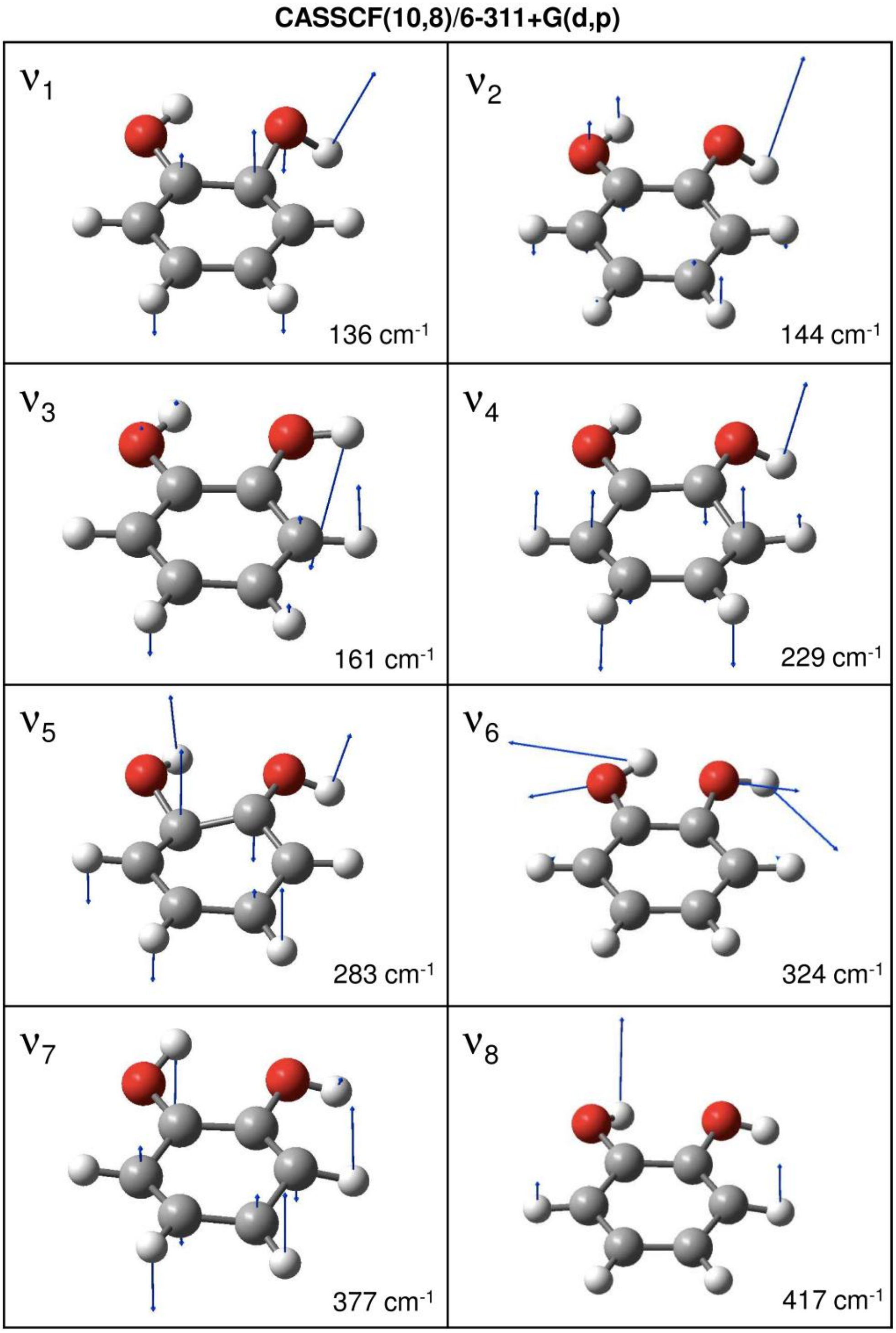

Fig. S7 Calculated harmonic frequencies for catechol in its S_1 state at the CASSCF(10,8)/6-311+G(d,p) level. The eight lowest frequency modes are presented (labelled ν_1 to ν_8). All eight vibrations exhibit significant mode-mixed character, including O-H torsion and in- and out-of-plane motions.

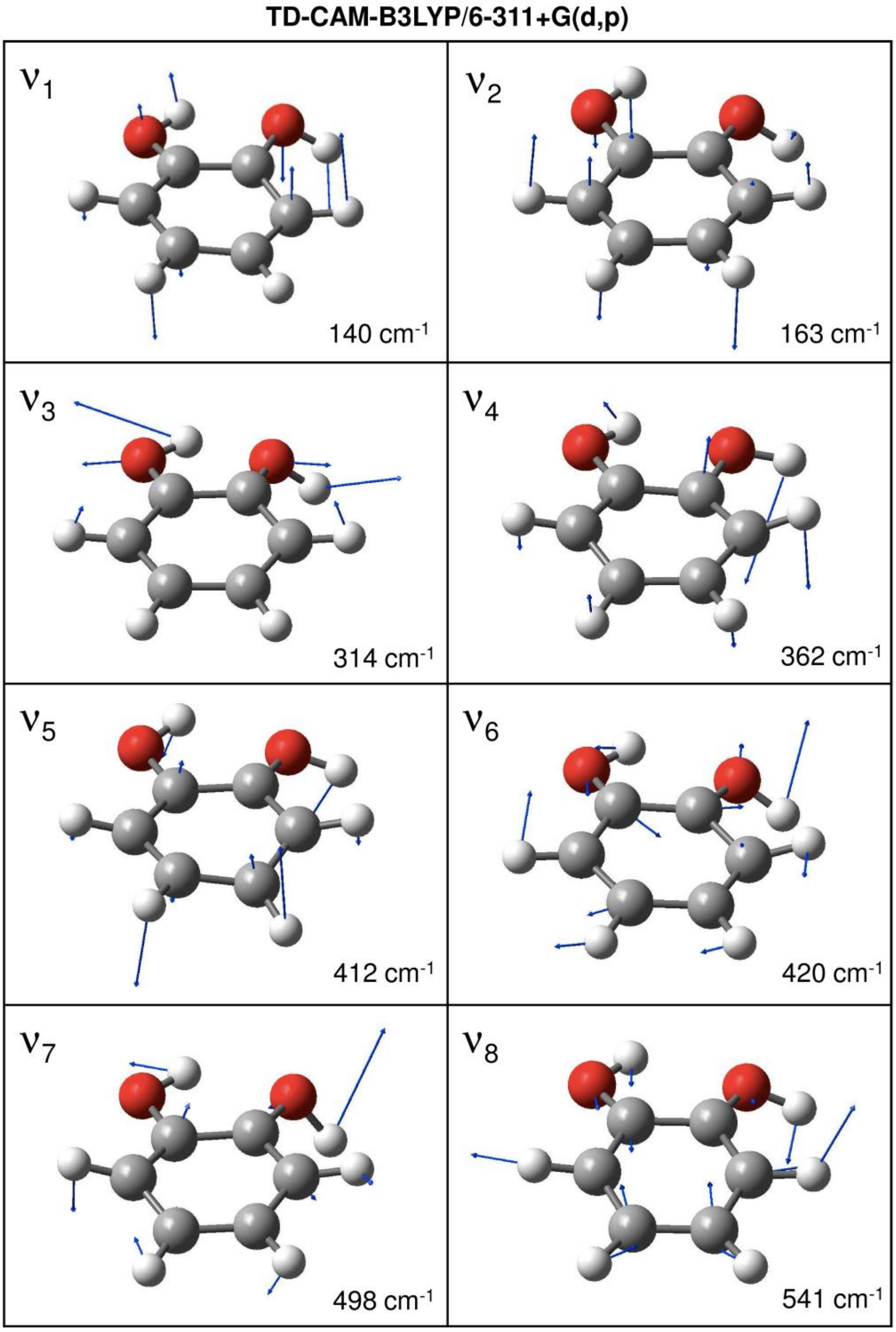

Fig. S8 Calculated harmonic frequencies for catechol in its S_1 state at the TD-CAM-B3LYP/6-311+G(d,p) level (frequencies were determined using a numerical frequency calculation). The eight lowest frequency modes are presented (labelled ν_1 to ν_8). As with the CASSCF(10,8)/6-311+G(d,p) calculated vibrations, all eight vibrations at the TD-CAM-B3LYP/6-311+G(d,p) level exhibit significant mode-mixed character, including O-H torsion and in- and out-of-plane motions.

S9. Calculated minimum energy geometries of catechol's S_1 state

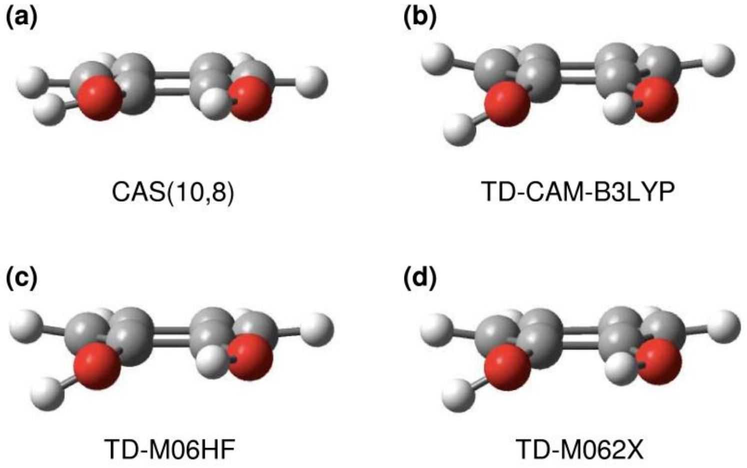

Fig. S9 Minimum energy geometries of catechol's S_1 state ($S_{1\ \mathrm{min}}$) at the (a) CASSCF(10,8) (b) TD-CAM-B3LYP (c) TD-M06HF and (d) TD-M062X levels of theory. All calculations utilised a 6-311+G(d,p) basis set.

Calculations of the minimum energy geometries for the S_1 state ($S_{1\ \mathrm{min}}$) were performed using the Gaussian 09 computational suite,[3] and are presented in Fig. S8. The structure calculated at the CASSCF(10,8)/6-311+G(d,p) level of theory is in good qualitative agreement with that reported in earlier studies by Gerhards *et al.*,[4] which also used the same (10,8) active space but with a smaller 6-31G(d,p) basis set. The 'free' O^1-H bond is calculated to lie at an angle of ~16° degrees out of the phenyl ring plane, compared to ~24° at the CASSCF(10,8)/6-31G(d,p) level.[4]

The structures determined using density functional response theory, with the CAM-B3LYP,[5] M06HF[6] and M062X[7] functionals, are in good agreement with each other. Reassuringly, these calculated $S_{1\ \mathrm{min}}$ structures are very comparable to that previously determined at the RI-CC2/aug-cc-pVTZ level by Ashfold and co-workers.[8] However, all response theory methods find that there is a significant out-of-plane distortion of the phenyl ring, as well as the C-O-H moieties, unlike the structure calculated at the CASSCF(10,8)/6-311+G(d,p) level. The precise origins of this discrepancy are currently unclear, although a lack of dynamic correlation effects in the CASSCF calculations may be one possible cause; further theoretical studies are required to investigate this in greater detail, but are beyond the scope on the present work. Nonetheless, both response theory and CASSCF calculations provide strong evidence that the $S_{1\ \mathrm{min}}$ structure of catechol is indeed non-planar.

S10. Determination of branching fractions (Γ)

The experimentally observed branching fraction (Γ) for S_2 driven O^1-H bond fission originating from tunnelling under the S_1/S_2 CI, at each excitation wavelength (λ) is determined using the time-resolved TKER spectra presented in Fig. 3 of the main article. Γ is formally defined as:

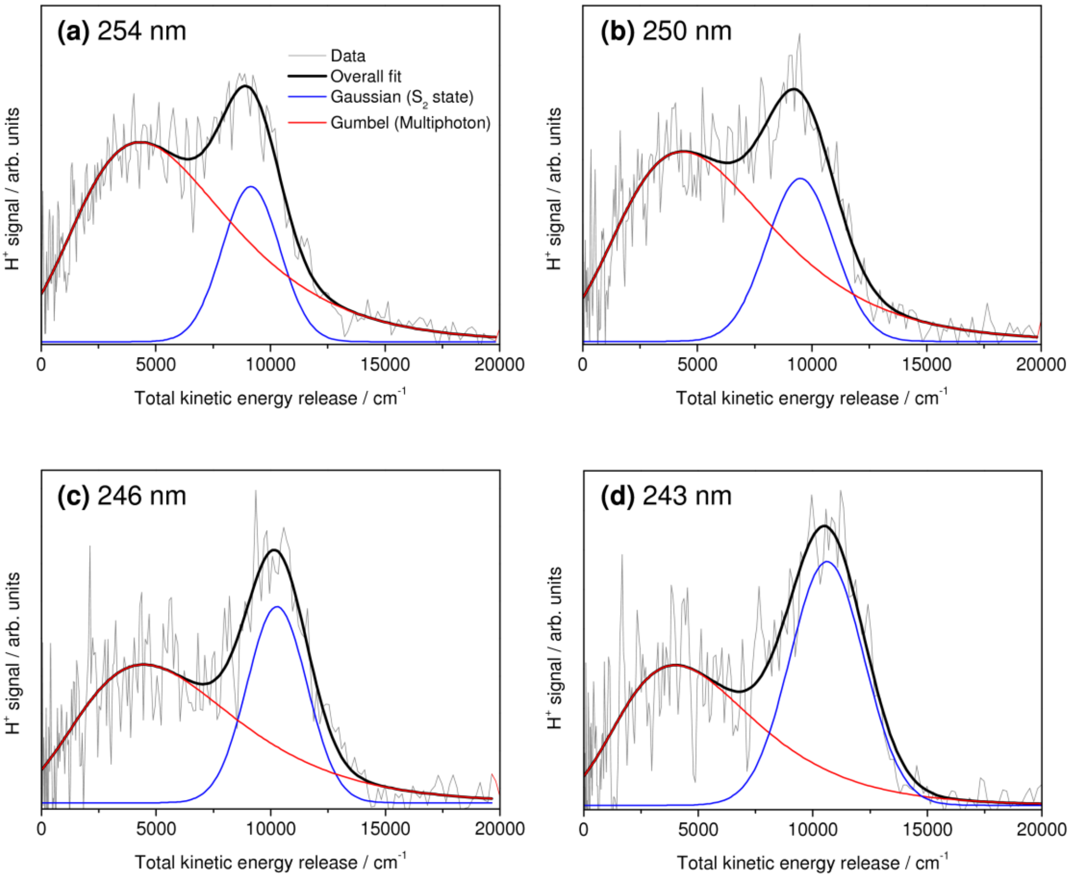

Fig. S10 Fits (black lines) to TKER spectra recorded at Δ*t* = 1 ps (grey line) at (a) 254, (b) 250, (c) 246 and (d) 243 nm. Fits are performed using eqn (S6) and the individual Gumbel (red lines) and Gaussian (blue lines) are also provided (see section S10 for details).

$$\Gamma = \frac{\gamma_1}{(\gamma_1 + \gamma_2)}, \qquad \text{(S5)}$$

where γ_1 and γ_2 are the total integrated signals associated with S_2 mediated O^1-H fission originating from tunnelling under the S_1/S_2 CI and direct dissociation along the S_2 surface, respectively.

For wavelengths between 254 – 243 nm, γ_1 is determined by integrating the signal difference between TKER spectra recorded Δt = 50 ps and 1 ps (see red shading in Fig. 3 of main manuscript). Over the same wavelength range, γ_2 is determined by first fitting the profile of the TKER spectra at Δt = 1 ps, $I(x)$, to sum of a Gaussian and an extreme value (Gumbel) distribution, which have the functionality:

$$I(x) = I_0 + \left[A\exp\left(-\frac{(x-\mu_1)^2}{2\sigma_1^{\,2}} \right) \right] + \left[B\exp\left(-\frac{(x-\mu_2)}{\sigma_2} \right) \exp\left\{ -\exp\left(-\frac{(x-\mu_2)}{\sigma_2} \right) \right\} \right], \qquad \text{(S6)}$$

where x is the TKER, I_0 is the baseline signal level, A is the amplitude of the Gaussian function, σ_1 and μ_1 are the width and centre of the Gaussian distribution, respectively, B is the amplitude of the Gumbel function, and σ_2 and μ_2 are the width and location parameters of the Gumbel distribution. The results of these fits are shown in Fig. S10 as solid black lines overlaid on top of the recorded TKER spectrum (grey line). The Gumbel function is used to model the underlying two-colour background signal arising from undesired multiphoton processes (red line), while the Gaussian models the remaining contribution of H^+ signal associated with ultrafast O^1-H fission dynamics resulting from direct excitation to the S_2 surface (blue line). Values for γ_2 are finally obtained by integrating the Gaussian component of these fits, which together with γ_1, ultimately enable a determination of Γ.

ESI References

1. S. W. Konijn, R. J. J. M. Steenvoorden, P. G. Kistemaker and T. L. Weeding, *J. Phys. Chem.*, 1994, **98**, 5399-5403.
2. E. R. E. Vanderhage, J. J. Boon, R. J. J. M. Steenvoorden and T. L. Weeding, *Anal. Chem.*, 1994, **66**, 543-550.
3. *Gaussian 09*, Revision A.02, M. J. Frisch, G. W. Trucks, H. B. Schlegel, G. E. Scuseria, M. A. Robb, J. R. Cheeseman, G. Scalmani, V. Barone, B. Mennucci, G. A. Petersson, H. Nakatsuji, M. Caricato, X. Li, H. P. Hratchian, A. F. Izmaylov, J. Bloino, G. Zheng, J. L. Sonnenberg, M. Hada, M. Ehara, K. Toyota, R. Fukuda, J. Hasegawa, M. Ishida, T. Nakajima, Y. Honda, O. Kitao, H. Nakai, T. Vreven, J. A. Montgomery, Jr., J. E. Peralta, F. Ogliaro, M. Bearpark, J. J. Heyd, E. Brothers, K. N. Kudin, V. N. Staroverov, R. Kobayashi, J. Normand, K. Raghavachari, A. Rendell, J. C. Burant, S. S. Iyengar, J. Tomasi, M. Cossi, N. Rega, J. M. Millam, M. Klene, J. E. Knox, J. B. Cross, V. Bakken, C. Adamo, J. Jaramillo, R. Gomperts, R. E. Stratmann, O. Yazyev, A. J. Austin, R. Cammi, C. Pomelli, J. W. Ochterski, R. L. Martin, K. Morokuma, V. G. Zakrzewski, G. A. Voth, P. Salvador, J. J. Dannenberg, S. Dapprich, A. D. Daniels, Ö. Farkas, J. B. Foresman, J. V. Ortiz, J. Cioslowski, and D. J. Fox, Gaussian, Inc., Wallingford CT, 2009.
4. M. Gerhards, S. Schumm, C. Unterberg and K. Kleinermanns, *Chem. Phys. Lett.*, 1998, **294**, 65-70.
5. T. Yanai, D. P. Tew and N. C. Handy, *Chem. Phys. Lett.*, 2004, **393**, 51-57.
6. Y. Zhao and D. G. Truhlar, *J. Phys. Chem. A*, 2006, **110**, 13126-13130.
7. Y. Zhao and D. G. Truhlar, *Theor. Chem. Acc.*, 2008, **120**, 215-241.
8. G. A. King, T. A. A. Oliver, R. N. Dixon and M. N. R. Ashfold, *Phys. Chem. Chem. Phys.*, 2012, **14**, 3338-3345.